

Dual Band MWIR/LWIR Focal Plane Array Test Results

August 1999

A. Goldberg

EO/IR Technology Branch, Army Research Laboratory, Adelphi, MD 20783

&

S. Wang, M. Sundaram, P. Uppal, and M. Winn

Advanced Technology Division, Sanders, A Lockheed Martin Company

Nashua, NH 03060

&

G. Milne and M. Stevens

Lockheed-Martin Electronics and Missiles

Orlando, FL 32819

ABSTRACT

We report the imaging test results of the first 2-color MWIR/LWIR 256×256 QWIP FPA with simultaneous integrating capability. The FPA studied contained stacked GaAs/AlGaAs QWIP structures with spectral peaks at $5.1 \mu\text{m}$ and $9.0 \mu\text{m}$. Normally incident radiation was coupled into the device using a diffraction grating designed to operate in both spectral bands. Each pixel is connected to the read-out integrated circuit by three bumps to permit the application of separate bias levels to each QWIP stack and allow simultaneous integration of the signal current in each band. We found the FPA to have high pixel operability, well-balanced response, good imaging performance, high optical fill-factor, and low spectral crosstalk. Data are presented on measurements of the noise-equivalent temperature difference of the FPA in both bands as functions of bias and temperature. We also present data on the sensitivity of this FPA to polarized light.

1.0 INTRODUCTION

Over the last few years, much effort has been invested in producing dual-band infrared (IR) imaging. Some of the motivations for dual-band IR imaging are enhanced detection of targets in clutter, the ability to distinguish between targets and decoys, and remote absolute temperature measurement. These efforts have produced infrared focal plane arrays (FPAs) operating at two wavelengths in the mid-wave infrared¹ (MWIR, 3 to $5 \mu\text{m}$) and the long-wave infrared² (LWIR, 8 to $12 \mu\text{m}$) as well as FPAs

¹J. Caufield, *et al*, "Simultaneous Integrating Staring Two Color IRFPAs," *Proc. 1997 IRIS Detector Specialty Group Meeting on Detectors*, p. 351 (1998).

²M. Sundaram, *et al*, "Advances in QWIP FPA (2-Color and 1-Color) Technology," *Proc. 1998 IRIS Specialty Group Meeting on Detectors*, p. 219 (1999).

Form SF298 Citation Data

Report Date <i>("DD MON YYYY")</i> 00081999	Report Type N/A	Dates Covered (from... to) <i>("DD MON YYYY")</i>
Title and Subtitle Dual Band MWIR/LWIR Focal Plane Array Test Results		Contract or Grant Number
		Program Element Number
Authors		Project Number
		Task Number
		Work Unit Number
Performing Organization Name(s) and Address(es) EO/IR Technology Branch Army Research Laboratory Adelphi, MD 20783 &		Performing Organization Number(s)
Sponsoring/Monitoring Agency Name(s) and Address(es)		Monitoring Agency Acronym
		Monitoring Agency Report Number(s)
Distribution/Availability Statement Approved for public release, distribution unlimited		
Supplementary Notes		
Abstract		
Subject Terms		
Document Classification unclassified	Classification of SF298 unclassified	
Classification of Abstract unclassified	Limitation of Abstract unlimited	
Number of Pages 17		

operating in both the LWIR and MWIR.³ In earlier efforts, the pixels of the individual colors were either not spatially registered or the outputs were read out sequentially (not simultaneously).

Recently, the Army Research Laboratory (ARL), in federation with several industry and academic partners, has developed the concept of the multi-domain smart sensor (MDSS).⁴ This conceptual or "technology demonstration" system is envisioned as a single unit combining both passive and active sensor components with advanced signal processing and aided target recognition (ATR) tools. Such a sensor would enhance the situational awareness on the battlefield in all ambient conditions by locating and classifying threats with increased effectiveness over existing systems. An integral part of the MDSS system is a dual-band infrared imager operating in the MWIR and LWIR bands. Such an imager would be advantageous over single-color IR cameras (either LWIR or MWIR) because it can operate in a wider range of ambient conditions and be more effective in defeating IR countermeasures such as smoke, camouflage, and flares. The MDSS program has supported research aimed at producing large-format, staring, dual-band FPAs. Both quantum well infrared photodetector⁵ (QWIP) and mercury-cadmium telluride (HgCdTe or MCT) technologies were investigated. This paper presents the results for the QWIP devices.

The quantum well infrared photodetector is made using GaAs and other III-V semiconductors, has been put forward as an alternative to the incumbent MCT devices for dual-band infrared FPAs. The QWIP detector structure has the advantage over an MCT detector in that the spectral response is relatively narrow so that a detector designed for the 8 to 10 μm wavelength band only detects light in that band with little or no "spectral crosstalk" with a detector in the 3 to 5 μm band. QWIPs have been designed and demonstrated to operate effectively at peak wavelengths as short as 3 μm to longer than 16 μm . Dual-band detector structures present no serious materials growth issues because, for the most part, the operating wavelengths are determined by the layer thicknesses, which are easily controlled with molecular beam epitaxy (MBE). In addition, the material growth and processing technology are much more mature in the III-V material systems relative to the II-VI materials like MCT, allowing for high operability of FPAs with uniform pixel-to-pixel response (which is the principal limitation of the performance of modern IR FPAs).

The principal disadvantages of QWIPs are their low single-pixel quantum efficiency relative to MCT and relatively high dark currents at temperatures near that of liquid nitrogen (77 K). The high dark current at 77 K necessitates cooling to temperatures around 65 K or below to obtain background-limited performance (BLIP) in LWIR QWIPs. Nevertheless, excellent IR imagery has been demonstrated with large format (640 \times 480 pixels) FPAs.

We will describe the fabrication and test results of a pixel-registered dual-band FPA designed to operate simultaneously in the MWIR and LWIR spectral regions. The results indicate that high-quality IR imagery can be obtained in both bands at operating temperatures lower than 65 K and that excellent MWIR performance can be achieved at an operating temperature of 90 K. In addition, the LWIR portion of the FPA is shown to have high sensitivity to the polarization state of the incident radiation, allowing

³ D. Scribner, J. Schuler, P. Warren, M. Satyshur, M. Kruer, "Infrared Color Vision: Separating Objects from Backgrounds," *Proceedings of the SPIE - Infrared Detectors and Focal Plane Arrays V*, Vol. 3379, p. 2 (1998).

⁴ H. Pollehn and J. Ahearn, "Multi-Domain Smart Sensors," *Proceedings of the SPIE, Infrared Technology and Applications XXV*, Vol. 3698, Orlando, FL (1999).

⁵ K. K. Choi, *The Physics of Quantum Well Infrared Photodetectors*, World Press, Singapore, (1997).

for additional information to be gathered from the scene as compared to FPAs made with the incumbent FPA technology.

2.0 FPA FABRICATION

2.1 Detector Array

Sanders, A Lockheed Martin Company, fabricated the detector array used in this effort. The two-color QWIP structures were grown MBE on 3 in-diameter semi-insulating (SI) GaAs substrates. The detector structures consisted of two active QWIP regions separated by heavily doped ohmic contact layers. The MWIR QWIP was designed to have maximal response at $4.7\ \mu\text{m}$, and the LWIR QWIP was designed to have peak response at $8.6\ \mu\text{m}$. The LWIR QWIP is a 20-period GaAs/ $\text{Al}_x\text{Ga}_{1-x}\text{As}$ multi-quantum well (MQW) stack with the GaAs well thickness and the Al composition (x) adjusted to yield the desired peak and spectral width. The MWIR detector was a similar 20-period MQW structure but the quantum wells were InGaAs grown pseudomorphically on the AlGaAs barrier material. The barriers consist of ~ 550 to $600\ \text{\AA}$ -thick undoped AlGaAs. The GaAs (InGaAs) wells are doped with Si to provide ground state electrons. Figure 1 shows the structure schematically. The two stacks are separated by an intermediate ohmic layer of doped GaAs. A bottom contact layer of doped GaAs below the MWIR QWIP and a top contact layer of doped GaAs above the LWIR QWIP, complete the detector structure. Two AlGaAs etch stop layers separated by a layer of undoped GaAs (called an isolator) are grown beneath the dual-QWIP structure. All the wafers had defect densities $< 100\ \text{cm}^{-2}$ after MBE growth.

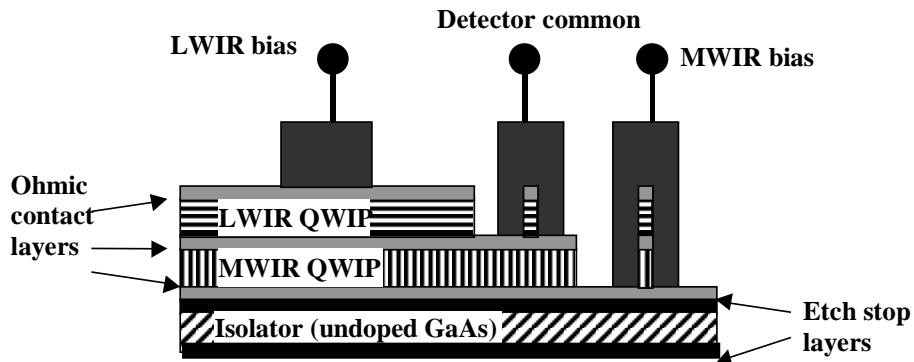


Figure 1. Schematic representation of the dual-band QWIP detector structure.

Two wafers were selected and subjected to a wafer-level 256×256 FPA (pitch = $40\ \mu\text{m} \times 40\ \mu\text{m}$, pixel = $39\ \mu\text{m} \times 39\ \mu\text{m}$) fabrication process using a stepper for all photolithography definitions and reactive ion etching (RIE) for all pattern printing. The process involved definition of an array of pixels, with the same grating pattern delineated on all pixels, and metal runs to each of the three ohmic contact layers in every pixel. The top etch stop layer ensures that the pixel is etched deep enough to be electrically isolated from its neighbors. The bottom etch stop layer is used in the substrate removal process following hybridization. The isolator layer (between the two etch stop layers) provides physical support to all the pixels in the thinned array. Figure 2 shows a micrograph of the processed detector array. A pattern of indium bumps (three/pixel) was then defined on the entire wafer.

The diffraction grating, the pattern of rectangles etched into the tops of the detector mesas, was designed to couple normally incident light into both QWIP structures. The grating is biperiodic, having two different periods orthogonal to each other. This creates two linear gratings that are each tuned to the

wavelengths of the detector material. The choice of linear gratings for the dual-band FPA is a compromise. It is known that for single-color QWIPs, a two-dimensional square grating has superior optical coupling performance compared to one-dimensional (linear) gratings.⁶ However, the coupling efficiency of square gratings is highly dependent on the wavelength of the incident light. A square grating designed to have maximum coupling at a wavelength of 9 μm will have its minimum coupling efficiency (near 0) at half the design wavelength (4.5 μm). Such a grating would be unsuitable for a MWIR/LWIR dual-band QWIP because the wavelengths of interest differ by nearly a factor of 2.

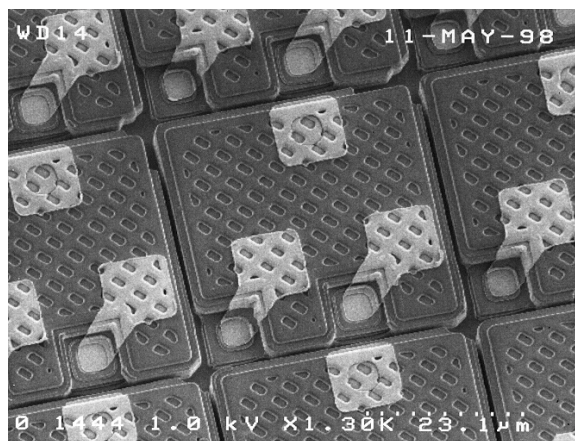


Figure 2. Section of two-color QWIP FPA prior to indium bump deposition, showing high optical fill factor, vertical sidewalls, and metal lines to each ohmic-contact layer.

Each wafer was diced to separate individual arrays; selected die were In bump bonded to a matching three bumps/pixel read-out integrated circuit (ROIC), wicked with epoxy, and backside thinned to remove the entire substrate. The detector-ROIC hybrid is mounted and wire bonded in a 68-pin leadless chip carrier with a calibrated temperature sensor diode. One die from each wafer is used as a single pixel test (SPT) device. This die is indium bump-bonded to a fanout, thinned and packaged as described above. Blackbody, noise, spectral, and I-V measurements were performed on an SPT from each wafer to qualify the FPAs from that wafer.

2.2. Read-out Integrated Circuit

Lockheed Martin Electronics and Missile Systems designed the ROIC. The simultaneous-integration windowing ROIC was fabricated using a 0.5- μm CMOS process. It is designed to consume less than 50 mW of power with a 5 V supply, employs a switched-capacitor frame snapshot architecture capable of frame rates up to 180 frames/s, and can provide variable bias for each color. The capacitance of the integration capacitor may be selected using a serial word command. In low gain mode, the capacitance of the charge well is 1 pF and in high gain mode the capacitance is 0.1 pF (well capacity 2.5×10^7 and 2.5×10^6 electrons, respectively for $V_{DD} = 5$ V).

The ROIC provides bias to the detectors in the following manner. The ohmic contact layer between the MWIR and LWIR QWIP structures is made common for all pixels. This detector common (DETCOM) voltage is then held above the main power bias for the ROIC chip (V_{DD}). Bias levels on the

⁶ J. Y. Anderson and L. Lundqvist, Appl. Phys. Lett. **59**, 857, (1991).

LWIR and MWIR sections are maintained using separate bias supplies connected to the top and bottom ohmic contact bumps of the detector pixels, respectively. The detector bias voltages need to be less than VDD. In this way, the LWIR structure is biased such that the electrons flow toward the substrate and in the MWIR portion of the detector, the electrons flow away from the substrate.

3.0 RESULTS AND DISCUSSION

3.1 Single Pixel Test Results

Single pixel tests were carried out at ARL on a detector array that was hybridized to a silicon fanout. The substrate of the detector array was not completely removed (as was done with the array hybridized to the ROIC). The spectral response, responsivity, D^* , and photoconductive gain were measured on several detectors. The measurements were carried out in an MTD-120 liquid nitrogen pour-fill dewar. The sample temperature was 78 K and the field of view (FOV) was equivalent to $f/2$.

The detectors were measured in a bias configuration similar to that of the ROIC. Separate connections were made to the top, intermediate, and bottom ohmic contact layers of each detector. The bias voltage was applied to the intermediate layer (detector common). The contact to the top layer was shorted to ground to measure the LWIR response; the contact to the bottom layer was shorted to ground to measure the MWIR response. Figure 3 shows Spectral response curves for a typical dual-band QWIP detector from this array.

The spectrum of the LWIR section of the detector exhibited many sharp peaks that appeared to be regularly spaced in energy. These are believed to be due to interference effects caused by the incomplete thinning of the detector substrate. The fringes are separated by an average of 50 cm^{-1} implying that the substrate thickness was $30 \mu\text{m}$. These fringes are not resolved in the spectrum of the MWIR detector.

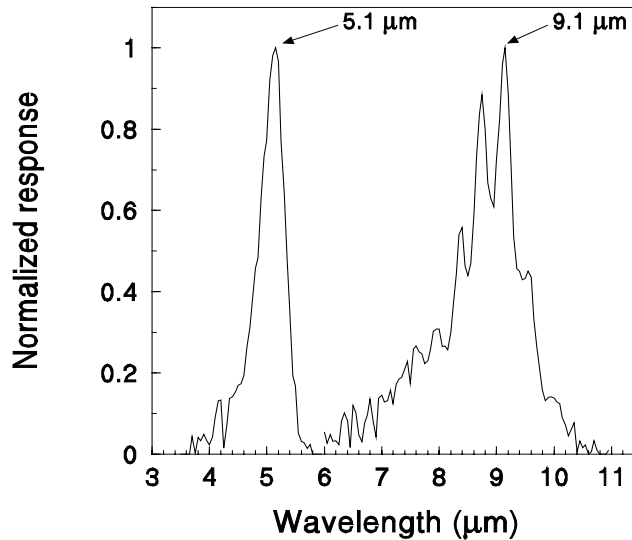


Figure 3. Normalized response spectra for the MWIR and LWIR sections of a typical dual-band QWIP detector.

Figure 4 shows the bias dependence of the peak responsivity (R_λ) and the conversion efficiency (defined as the product of the quantum efficiency and the photoconductive gain) for a typical device. The bias is relative to the detector common. The LWIR section shows a distinct maximum in responsivity at approximately 1.5 V, whereas the responsivity of the MWIR section increases monotonically with bias. The photoconductive gain was calculated from the detector bias current, the noise, and the dynamic resistance using the expression

$$g = \frac{1}{4eI_d} \left(\frac{I_n^2}{R_{dyn}} - J_n^2 \right) \quad (1)$$

where e is the electronic charge, I_d is the bias current, I_n is the measured noise density (A/ $\sqrt{\text{Hz}}$) of the detector, k is Boltzmann's constant, T is the device temperature, R_{dyn} is the dynamic resistance, and J_n is the measurement system noise density. At a temperature of 78 K and a 295 K background (f/2 aperture), the measured noise of the detector was well above that of the system for the LWIR portion of the device. Figure 5 shows the results of the calculation of the photoconductive gain for a typical LWIR detector.

Figure 6(a) shows the peak D^* (D^*_{λ}) as a function of bias for a typical LWIR (circles) and MWIR (squares) at a device temperature of 78 K. The detector noise for the MWIR structure was comparable to or lower than the system noise (1.53×10^{-14} A/ $\sqrt{\text{Hz}}$). Therefore, the D^*_{λ} values for the MWIR detector shown in Figure 6(a), represent lower limits to the actual values of D^*_{λ} . The photoconductive gain for the MWIR structure could not be reliably calculated from the 78-K detector noise data, but we expect that it will be approximately the same as that for the LWIR structure.

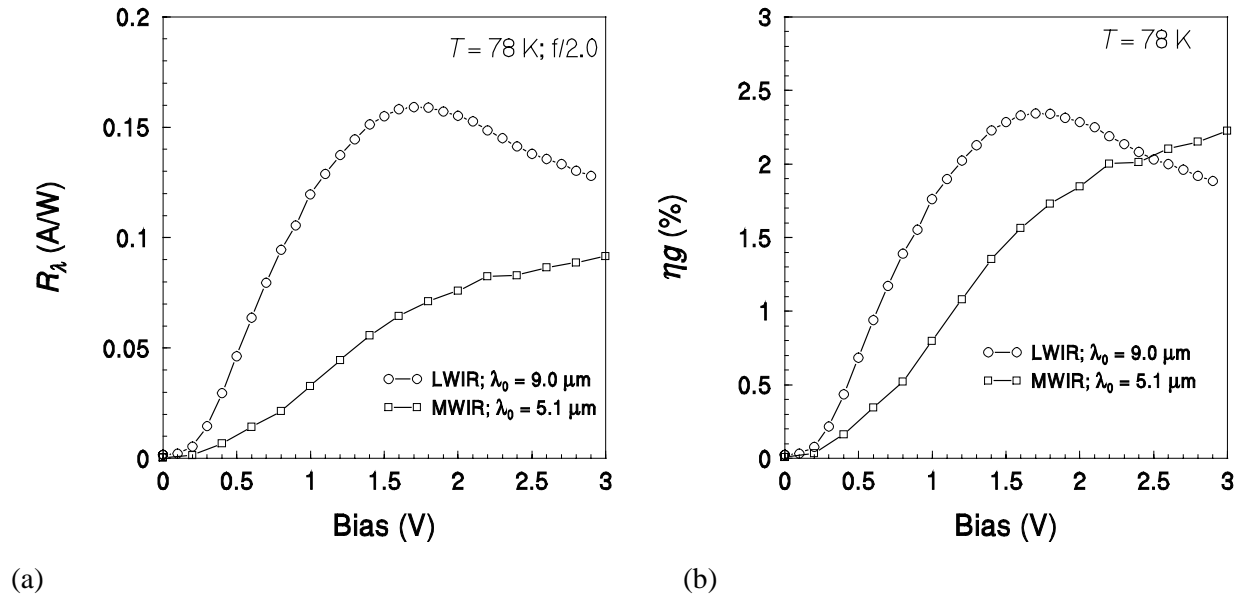


Figure 4. Peak responsivity (a) and conversion efficiency (b) for the LWIR and MWIR portions of the dual-band QWIP as a function of detector common bias.

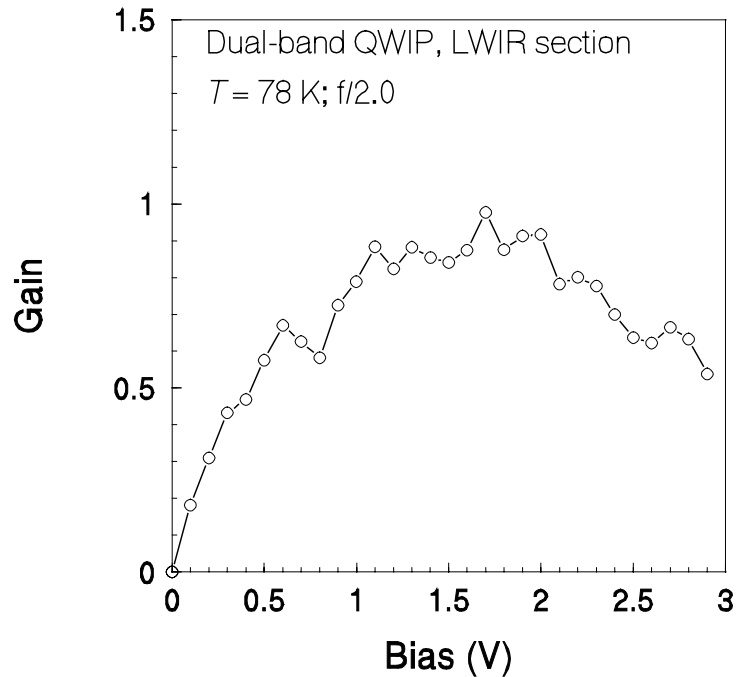
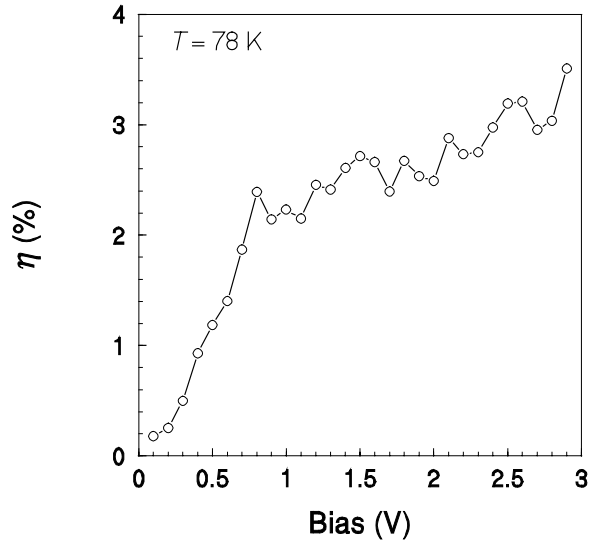
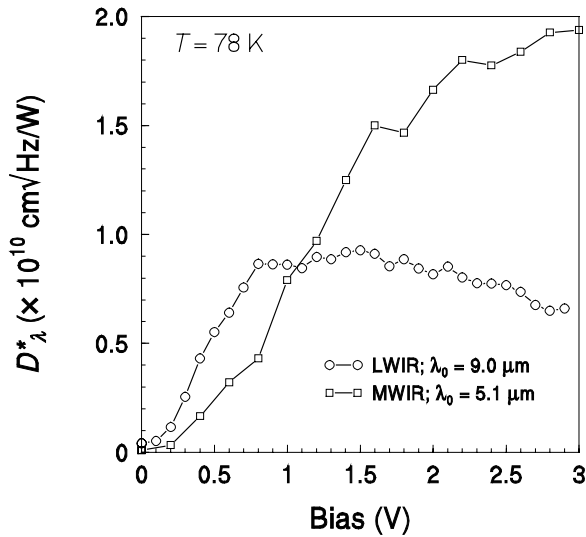


Figure 5. Photoconductive gain vs. detector common bias for the LWIR portion of the dual-band QWIP.

Figure 6 shows the quantum efficiency of the LWIR part of the dual band detector as a function of bias. The quantum efficiency is between 2 and 3 percent over the normal operating bias range. Given this value of quantum efficiency, a background temperature of 295 K, and an FOV of f/2, we would expect the temperature for background-limited performance (BLIP) for this device to be 62 K. The low quantum efficiency of this device relative to previously reported QWIP detectors⁷ can be attributed to the (effectively) linear diffraction grating used to couple light into the structure.

We found the conversion efficiency of the MWIR portion of the detector to be approximately 2 percent at a bias of 2 V. The gain is believed to be on the order of unity (as was the case for the LWIR structure) so that the quantum efficiency of the MWIR device is also approximately 2 percent. Because of the relatively lower dark current for the MWIR detector (compared to an LWIR detector of equivalent quantum efficiency), we expect the BLIP temperature of the MWIR device to be 102 K.

⁷ N.C. Das, K.K. Choi, A. C. Goldberg, A. La, M. Jhabvala, R.B. Bailey, and K. Vural, Fabrication and evaluation of 11.2 and 16.2 μm cutoff C-QWIP arrays, *Proceedings of the SPIE, Infrared Technology and Applications XXV*, Vol. 3387, Orlando, FL (1999).



(a)

(b)

Figure 6. Peak D^* for the LWIR (circles) and MWIR (squares) portions of the dual band QWIP (a), and peak quantum efficiency vs. bias for the LWIR portion of the dual band detector at an operating temperature of 78 K (b).

3.2 FPA Tests

We conducted the tests on the dual-band array were done at ARL with the FPA installed in a liquid helium flow-through cryostat (Lakeshore MTD-150). The input clock and bias signals as well as the output pixel data were provided and collected by a configurable FPA drive electronics unit made by SE-IR Corporation. The pixel signals were digitized using 12-bit analog to digital converters (A/DC) capable of data rates up to 12 megapixels/s. The cryostat was equipped with an internal, cooled aperture wheel allowing for operation of the FPA under a wide range of background flux conditions (including 0-background). Table 1 shows the bias values used to run the FPA. The frame rate used for tests was typically 60 Hz when viewing the blackbody source. This allowed for integration times as short as 80 μ s and as long as 16 ms. For the dark current tests, frame rates as low as 1 Hz and integration times as long as 800 ms were used.

Under typical tactical background conditions (background temperature \sim 300 K, f/2.0 to f/3.0) the photon flux in the MWIR portion of the spectrum covered by this FPA is approximately 10^9 photons/cm²/s while that for the LWIR band is about an order of magnitude higher. Therefore, the MWIR portion of the array was nearly always run in the “high gain” mode with charge well capacitance of 0.1 pF while the LWIR portion was run in “low gain” mode with its charge well capacitance being 1.0 pF.

Table 1. Bias functions on the dual-band FPA and the values used in this work.

Bias Name	Function	Values Used (V)
VDD	Main power voltage for the ROIC.	5.00
DETCOM	Detector common voltage applied to the intermediate ohmic contact layer.	5.50 – 6.50
DIBIAS1	Provide bias to the “top” ohmic contact layer. Used to bias the LWIR device.	3.40 – 4.40
DIBIAS2	Provide bias to the “bottom” ohmic contact layer. Used to bias the MWIR device.	2.00 – 3.00

The bias that is actually applied to the MWIR and LWIR sections of the detector array depends on all of the values given in Table 1. For the LWIR detector the bias is given by

$$LWBias = \{DETCOM - VDD\} + \{3.90 - DIBIAS1\} \text{ volts} \quad (2)$$

and the bias on the MWIR detector is

$$MWBias = \{DETCOM - VDD\} + \{3.90 - DIBIAS2\} \text{ volts.} \quad (3)$$

3.2.1 Dark Current and BLIP Temperature

For dark current measurements, we placed the 0 field-of-view cold stop in front of the FPA. The current was measured by integrating charge from the detectors for as long a time as necessary to fill the integration capacitor approximately halfway to saturation. A number of frames (typically 50) were then collected and averaged. The current was then calculated using

$$I = \frac{1}{\tau} NC_i G_{AD} \quad (4)$$

where N is the number of counts in the A/D (from 0 to 4095), C_i is the capacitance of the integration capacitor, G_{AD} is the gain of the A/D (V/count), and τ is the integration time. Similar data were collected with the shutter open ($f/2.5$ aperture) to measure the sum of the dark current and photocurrent. Figure 7 shows the results of these measurements. If we define the BLIP temperature as the temperature at which the dark current and the background-induced photocurrent are equal, then the LWIR array is BLIP below approximately 65 K and the MWIR array is BLIP below approximately 95 K. The data agree well with the values predicted from single-pixel tests described above.

The dark-current data follow the expected exponential dependence on temperature with thermal activation energies of 226 meV for the MWIR structure and 120 meV for the LWIR part of the array. These energies correspond to wavelengths of 5.48 μm and 10.32 μm for the MWIR and LWIR structures, respectively. Figures 8 and 9 show the histogram and spatial distributions of the thermal activation energies for the LWIR and MWIR portions of the FPA. The mean activation energies were 119.3 ± 3.0 meV and 226.3 ± 9.97 meV, corresponding to a nonuniformities in activation energy of 2.5% and 4.4% for the LWIR and MWIR arrays, respectively. However, since the dark current depends exponentially on the activation energy, these small variations in activation energy caused the dark current to vary by more than a factor of 2 across the FPA. The nonuniformity of the activation energy (and therefore, the dark current) is a major limiting factor in operating the QWIP FPA in the dark-current limit. At temperatures above the BLIP temperature, the large variation in dark current limits the gain that can be applied to the output

signals to a low value. Under these conditions, the span of output values covers the entire range of the A/D.

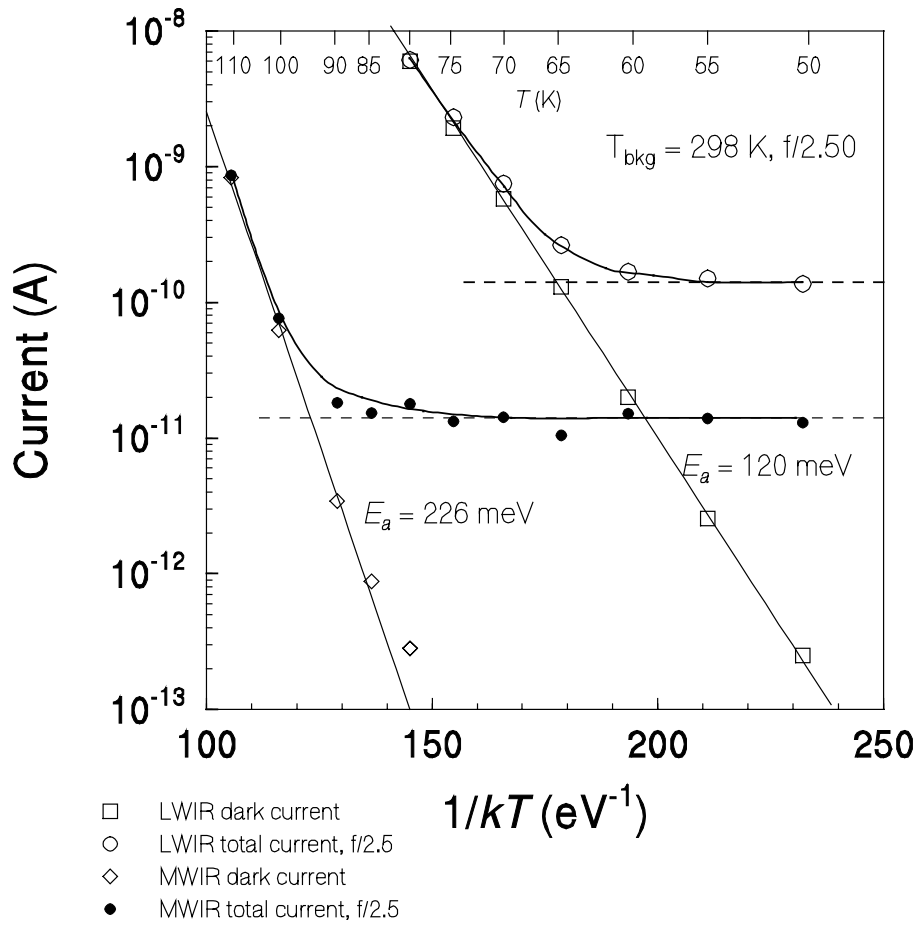


Figure 7. Mean dark current and total current for the MWIR and LWIR portions of the dual-band FPA. The background temperature was 298 K (25° C). The bias levels were 1.0 V for the LWIR and 2.0 V for the MWIR.

To operate effectively at high temperatures, the variation in dark current should be no more than that of the photocurrent (5 percent or less). For a small change in activation energy δE_a , the corresponding change in dark current is $\delta I_d / I_d = -\delta E_a / kT$ where T is the operating temperature. To achieve a dark current uniformity of 95 percent or better at 77 K, the activation energy must vary by no more than 0.33 meV or 0.275 percent. The observed variation in activation energy is an order of magnitude above this level.

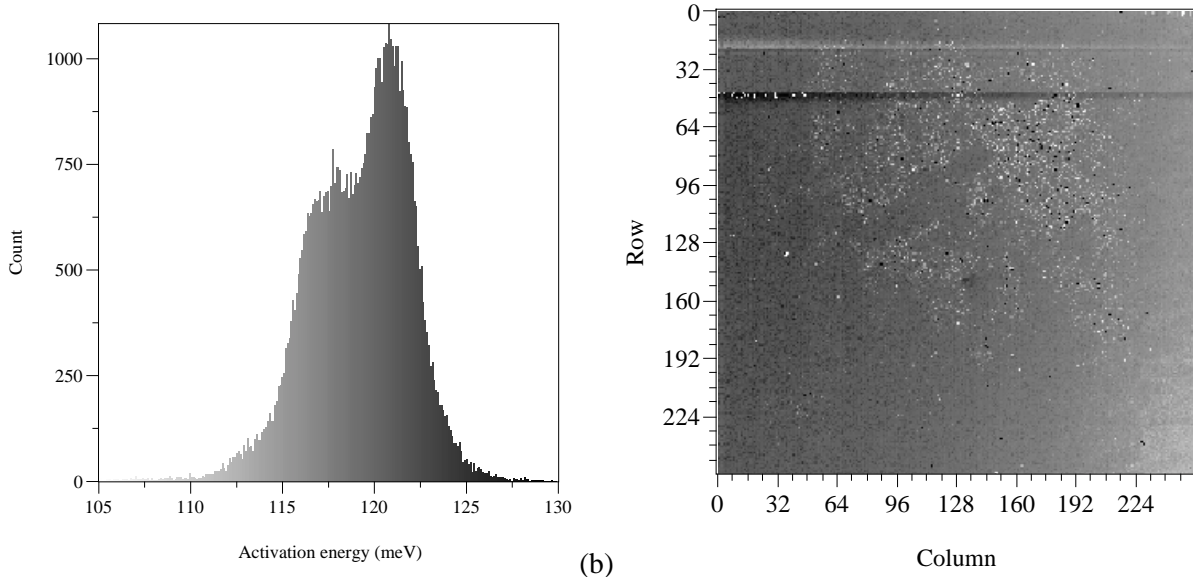


Figure 8. Histogram (a) and image (b) of the distribution of thermal activation energies for the LWIR pixels of the dual-band FPA. The mean activation energy is 119.3 ± 3.0 meV.

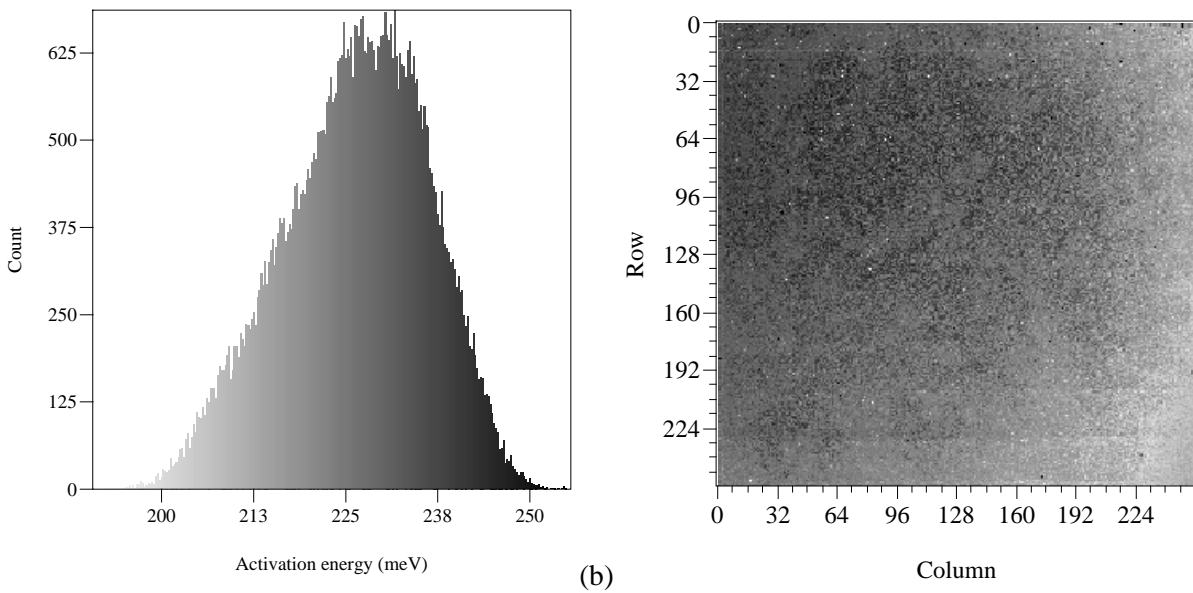


Figure 9. Histogram (a) and image (b) of the distribution of thermal activation energies for the MWIR pixels of the dual-band FPA. The mean activation energy is 226.3 ± 9.97 meV.

The images in Figures 8 and 9 show that the activation energy decreases monotonically from left to right across the FPA for both the LWIR and MWIR arrays. This behavior is most likely indicative of variations in the material growth parameters (growth rates and/or alloy composition) across the chip. A substantial reduction in such nonuniformities is one factor that may allow for operation of QWIPs at higher temperatures.

3.2.2 Imaging Performance, Operability, and Uniformity

The noise equivalent temperature difference (NE Δ T) was calculated from uncorrected imagery of an extended-area blackbody at different temperatures. The raw data consisted of many (usually 64) consecutive frames collected into a single file using a framegrabber built into the PC that operates the IR camera electronics. The data was then analyzed using the NVESD 3-D noise model⁸ to obtain the various components of NE Δ T. The data was taken at blackbody temperatures covering a 12 °C range in temperature from 20 °C to 32 °C; the calibration temperatures were defined as 22 °C and 30 °C. The data from each of the two bands was analyzed separately. Data were taken under a wide variety of operating conditions (bias levels) and at device temperatures ranging from 50 to 110 K.

We found that, under BLIP conditions, we could make the FPA performance relatively independent of the bias on the detectors by shortening or lengthening the integration time as needed to get the signals to cover most of the A/D range for a reasonable change in background temperature (~10 °C). Above the BLIP temperature, the large variation in output current made it difficult to find good operating conditions. In particular, in the temperature range between 65 and 70 K, the short integration times mandated by the relatively high dark currents in the LWIR part of the FPA also degraded the performance of the MWIR portion of the device. At temperatures of 70 K and above, it was impossible to operate the LWIR array and so the operating conditions were optimized for best MWIR performance.

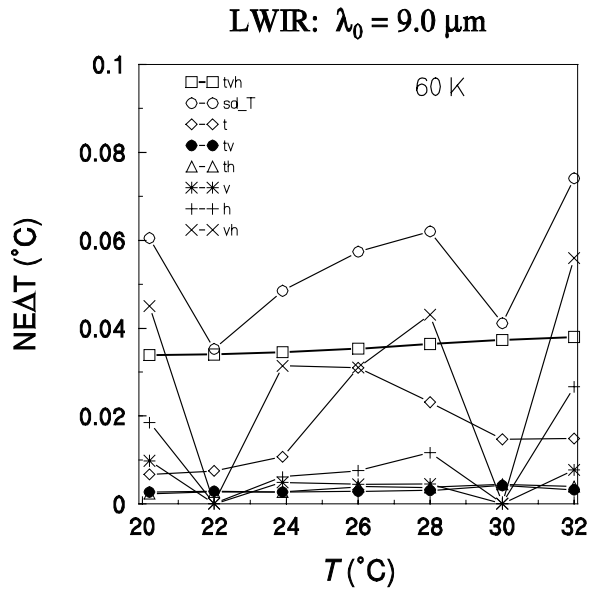
Figure 10 shows the 3-D noise components of NE Δ T for the LWIR (a) and MWIR (b) portions of the FPA at an operating temperature of 60 K. The integration time used was 8.0 ms, the LWIR bias was 1.0 V, and MWIR bias was 2.0 V. The temporal NE Δ T (N_{tvh}) was found to be approximately the same in both bands at about 32 mK. For the operating conditions described above, Figure 11 shows the histogram and image of the conversion efficiency of the LWIR array and Figure 12 shows those for the MWIR array. The imaging performance properties are summarized in Table 2 below.

Table 2. Performance properties of the dual-band MWIR/LWIR FPA at T=60 K.

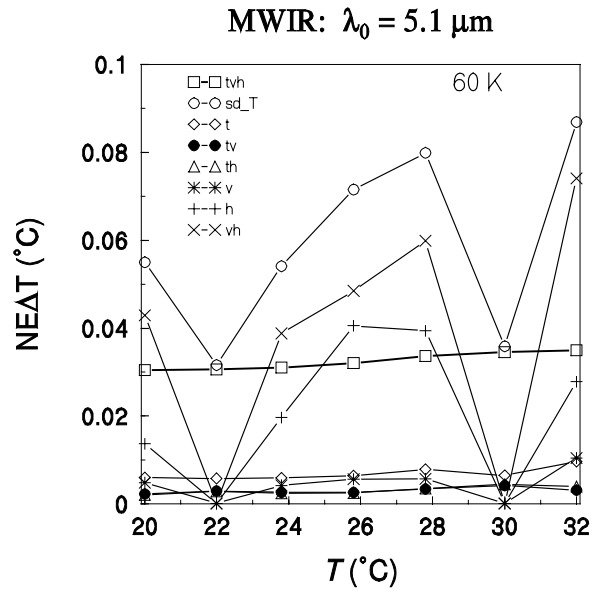
Band	Bias (V)	Mean Temporal NE Δ T (mK)	Mean Conversion Efficiency (%)	Pixels with Response Outside $\pm 10\%$ of Mean	Pixels with Response Outside $\pm 20\%$ of Mean
LWIR	1.00	34	2.61 \pm 0.119 ($\pm 4.56\%$)	229 (0.35%)	121 (0.18%)
MWIR	2.00	30	1.91 \pm 0.130 ($\pm 6.82\%$)	6346 (9.7%)	170 (0.26%)

The magnitude of the conversion efficiency as well as the pixel-to-pixel uniformity of the response are significantly better in the LWIR than in the MWIR. In both bands, the operability of the array is excellent with greater than 99.7 percent of the pixels having values of conversion efficiency within 20 percent of the mean. The fixed-pattern noise is, as expressed by the value of N_{vh} in the 3-D noise, is significantly larger in the MWIR data as opposed to that for the LWIR array. This is probably due to the higher nonuniformity of response in the MWIR array relative to that of the LWIR array.

⁸J. D'Augustino and C. Webb, "3-D Analysis Framework and Measurement Methodology for Imaging System Noise," in *Infrared Imaging Systems: Design, Analysis, Modeling and Testing II*, G. Holst, Editor, *Proceedings of the SPIE* Vol. 1488, 110-121 (1991).

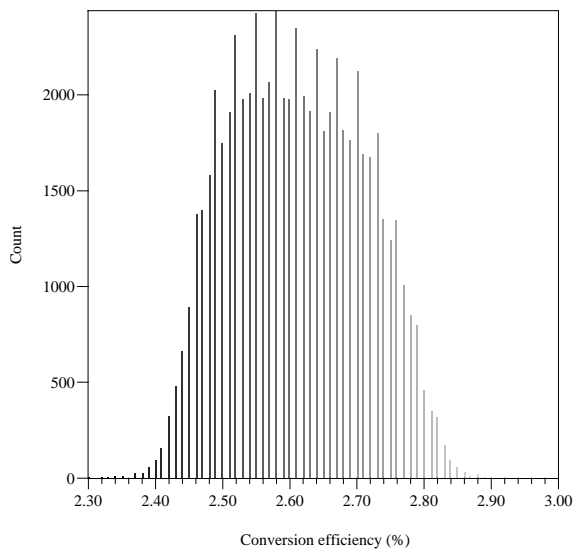


(a)

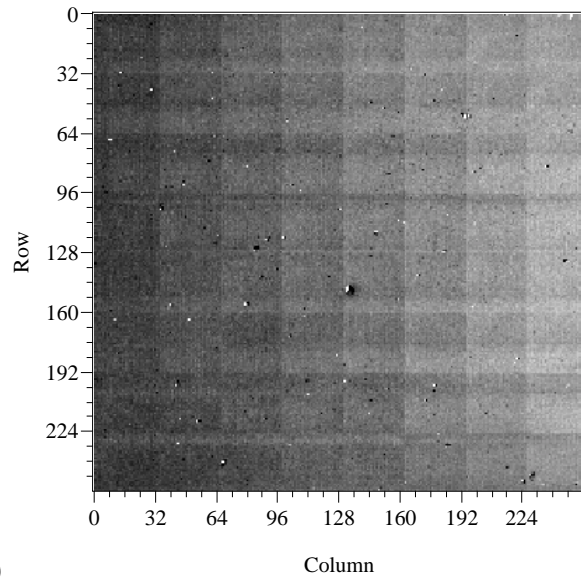


(b)

Figure 10. 3-D noise components as a function of background temperature for the LWIR array (a) and the MWIR array (b) at a device temperature of 60 K. The integration time was 8.0 ms, the LWIR bias was 1.0 V, and LWIR bias was 2.0 V.



(a)



(b)

Figure 11. Histogram (a) and grayscale image (b) of the conversion efficiency (quantum efficiency-gain product) for the LWIR part of the FPA.

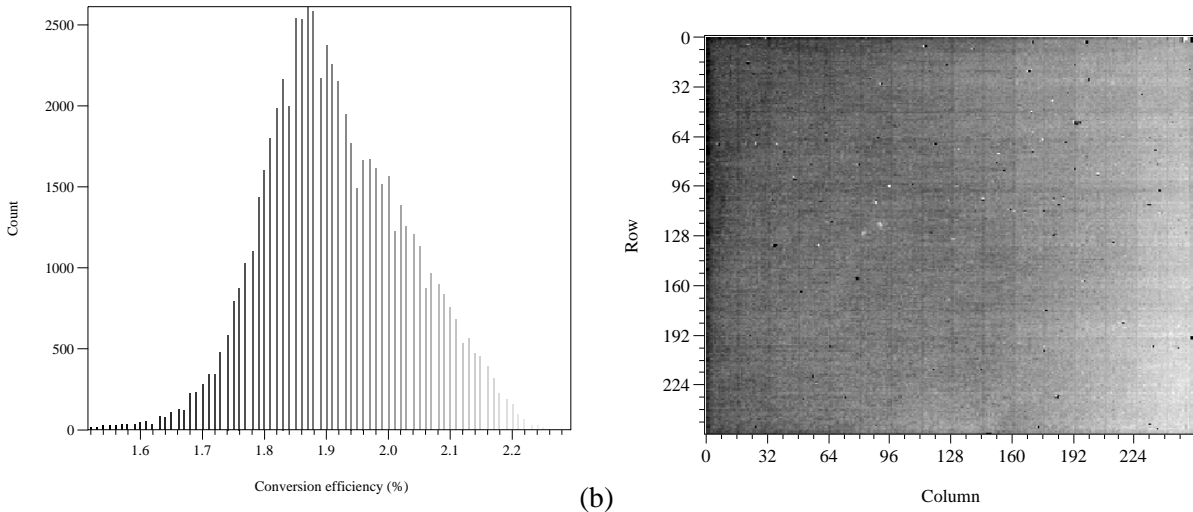


Figure 12. Histogram (a) and grayscale image (b) of the conversion efficiency (quantum efficiency-gain product) for the MWIR part of the FPA.

Figure 13 shows the results of measurements of temporal NE Δ T as a function of operating temperature. Below 65 K, the arrays from both bands had similar values of NE Δ T (between 30 and 40 mK). However, once the device temperature was higher than the BLIP temperature, the NE Δ T rose dramatically in both bands. The NE Δ T performance of the MWIR array degraded because short integration times were needed to keep the LWIR portion of the FPA from saturation (it was not possible to control the integration times for each band independently). At temperatures above 70 K, the operating conditions were optimized for the MWIR band. The NE Δ T was approximately 30 mK for temperatures less than 90 K; at temperatures above 90 K, the dark current becomes dominant in the MWIR device, thus causing the NE Δ T to rise sharply.

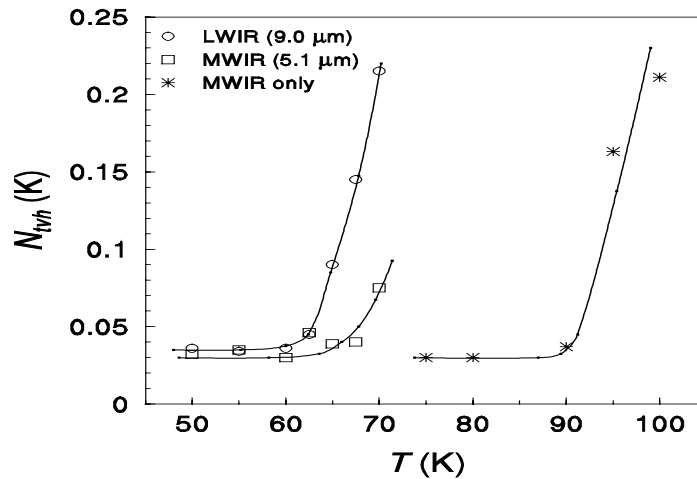
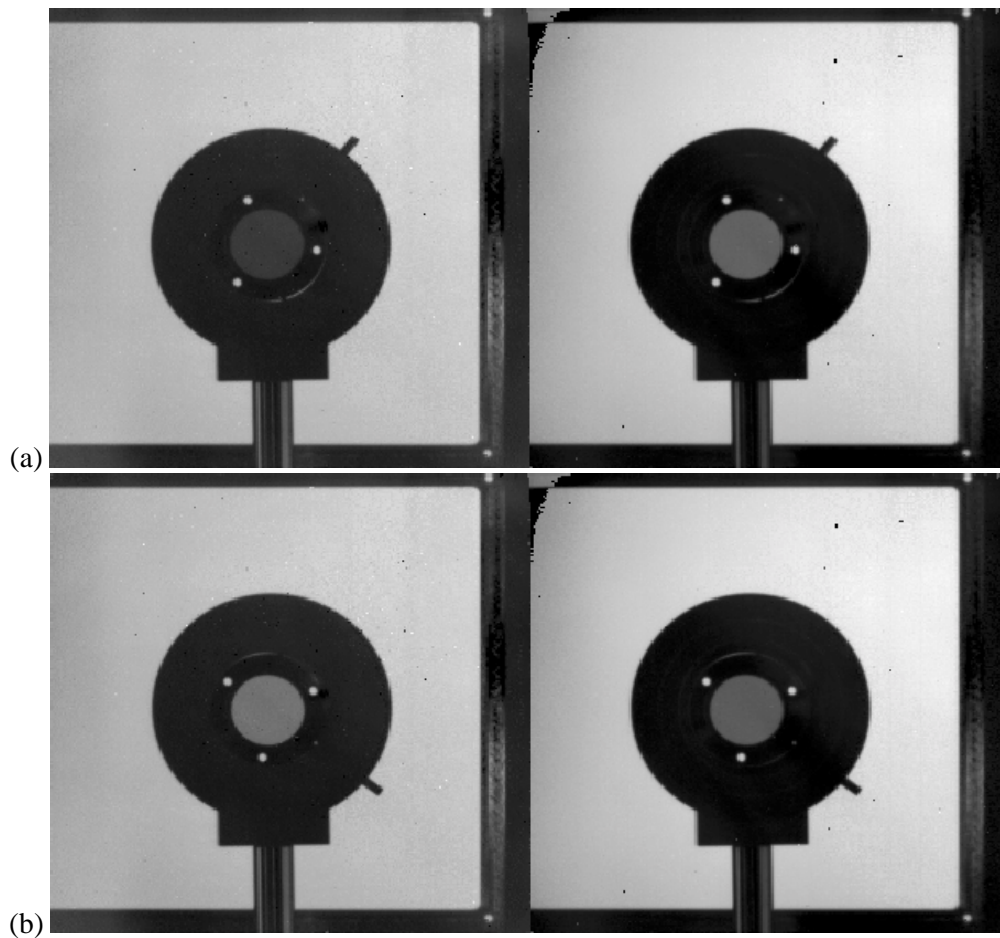


Figure 13. Mean temporal NE Δ T (N_{tvh}) as a function of operating temperature for the dual-band FPA. The circles and squares are the values of NE Δ T measured when operating conditions were optimized for running both bands simultaneously, the stars show the values of NE Δ T measured when the conditions were optimized for the MWIR array alone. The lines are simply guides to the eye.

3.2.3 Sensitivity to Polarized Light

A wire-grid polarizer was placed in front of the extended-source blackbody set at a constant temperature (25 °C) and imaged at different polarization angles. The results of this experiment are shown in Figures 14 and 15. Figure 14 shows simultaneous, side-by-side LWIR and MWIR images of the polarizer at angles of 40° (a), 130° (b), and 220° (c). Note that the LWIR shows a significant change in the number of photons detected as a function of the polarization of the incident light; the MWIR signal changes very little, if at all.

Figure 15 is a graph of the variation of output signals for the LWIR and MWIR arrays as a function of polarization angle. We see that the intensity has maxima near polarization angles of 130° and 310° and minima at 40° and 220°. The variation in intensity was found to be equivalent to a change in background temperature of 3 °C. The MWIR array does show a small (but observable) modulation of response with polarization angle. This modulation has maxima at the same angles that the LWIR response has minima. This result is a consequence of the orientation of the diffraction grating pattern on the pixels shown in Figure 2. The grating pattern is tilted at an angle of 45° relative to the major axes of the detector array. It is known that the maximum grating efficiency occurs for light polarized parallel to the “lines” of the grating. For the LWIR detector these angles are 135° and 315°, while for the MWIR array the angles are 45° and 225°. These are, in fact, the polarization angles at which the maxima occur.



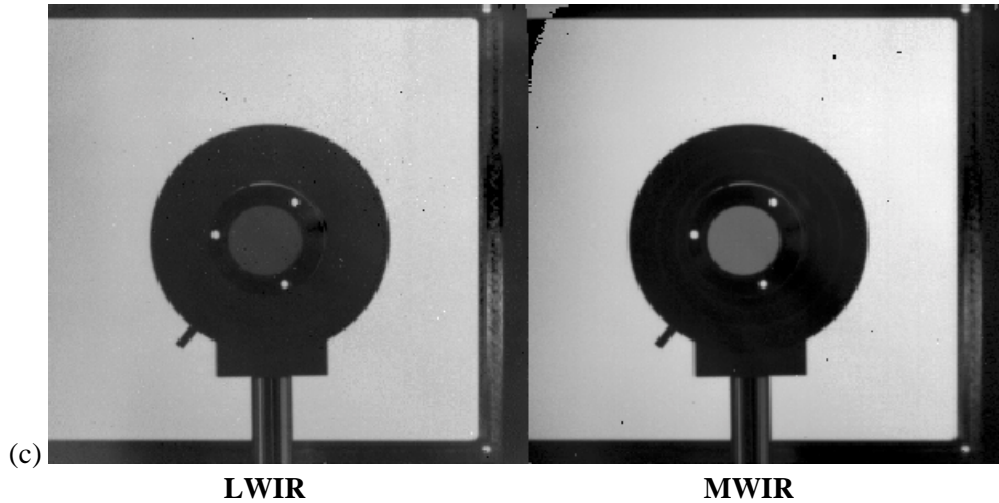


Figure 14. Simultaneous dual-band images of an infrared wire-grid polarizer at polarization angles of 40° (a), 130° (b), and 220° (c). The background is an extended-area blackbody set at a temperature of 25°C .

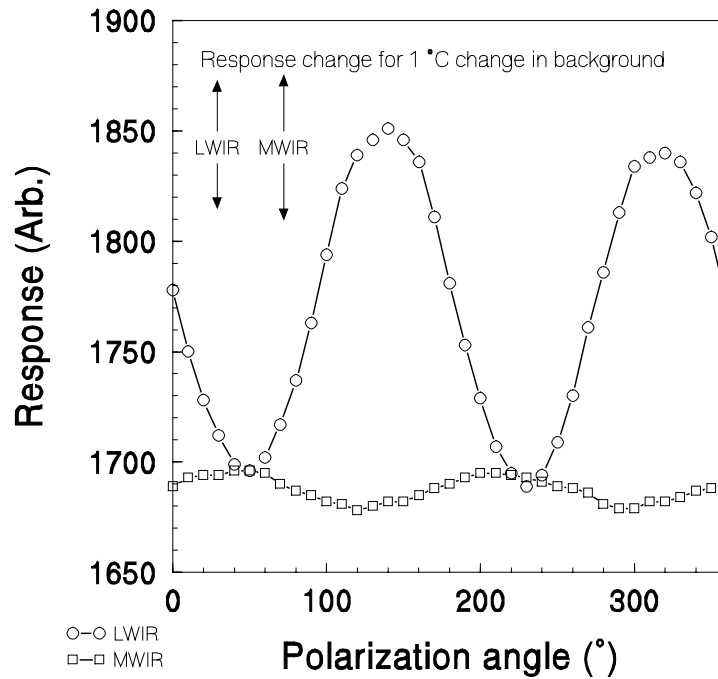


Figure 15. Response vs. polarization angle for the LWIR (circles) and MWIR (squares) portions of the dual-band FPA. The arrows show the change in response for a 1°C change in background temperature.

The results of the polarization tests imply that the MWIR light is not being coupled efficiently into the QWIP structure. The coupling in the LWIR, while less than that seen using two-dimensional

gratings, is significantly better than that in the MWIR section of the FPA. It appears, therefore that the bulk of the optical coupling that did occur in the MWIR portion of the FPA is due to light scattering from the edges of the pixels and/or grating features and not from resonant diffraction effects. The issue of efficient coupling in both wavelength bands needs to be addressed in order to enhance the performance of future dual-band FPAs.

4.0 SUMMARY AND CONCLUSION

We have shown imaging test results on a simultaneously integrating pixel-registered dual-band FPA operating in the MWIR (peaked at 5.1 μm) and LWIR (peaked at 9.0 μm) wavelength bands. The array was found to have excellent operability (>99.7 percent) and good imaging performance in both bands for temperatures less than 65 K. The temporal NE Δ T was found to be approximately 32 mK in both bands below 65 K and approximately 30 mK for the MWIR band for temperatures less than 90 K. We have shown that the LWIR array exhibits strong sensitivity to the polarization of the incident light, while the polarization sensitivity of the MWIR is approximately an order of magnitude weaker. The polarization sensitivity is due to the presence of a linear diffraction grating for each color. The lack of polarization sensitivity of the MWIR array was thought to be due to either: (a) the inefficiency of the MWIR part of the grating, and/or (b) the relatively long distance of the MWIR QWIP active layers from the grating structure. The results of these experiments will be used to improve the performance of future dual-band FPAs. In conclusion, Figure 16 shows an image acquired with the dual-band FPA described in this paper. It is notable that the flame is more prominent in the MWIR image than in the LWIR image.



Figure 16. Dual-band image of a person holding a lighter.

ACKNOWLEDGMENTS

We gratefully acknowledge the assistance of S. Kennerly, J. Little, D. Beekman, and W. Beck of ARL. The ROIC used for this work was designed and fabricated under the Advanced Multiple Quantum Well Technology (AMQWT) program funded by the Air Force Research Lab, contract number F08630-96-C-0083, managed by Mr. David Hayden and Mr. John Winterberger. We would also like to acknowledge the support of Dr. Walt Dyer and LTC Buckley of the Ballistic Missile Defense Organization.